TECHNICAL ARTICLE

Microstructural characterization of NiTi shape memory alloy produced by rotary hot forging

P. Rodrigues,[1,a)] F. M. Braz Fernandes,[1] A. S. Paula,[2,3] J. P. Oliveira,[1] S. B. Ribeiro,[4] E. N. Texeira,[4] and N. Schell[5]

[1]*CENIMAT, Faculdade de Ciências e Tecnologia, Universidade Nova de Lisboa, Portugal*
[2]*Mechanical Engineering and Materials Department-SE-4, Instituto Militar de Engenharia–IME, Brazil*
[3]*Metallurgical Engineering Post-Graduation Program (PPGEM), Universidade Federal Fluminense (UFF), Brazil*
[4]*Centro Universitário de Volta Redonda – UNIFOA, Brazil*
[5]*HZG, Geesthacht, Germany*

(Received 16 October 2016; accepted 26 April 2017)

The thermomechanical processing of NiTi shape memory alloys usually involves several steps of hot and/or cold deformation. The present work presents the structural characterization of a Ni-rich NiTi alloy bar, produced by vacuum-induced melting and thermomechanical processing in laboratory scale, aiming at massive production in the future. This study focused on the first step of hot working at 800 °C during rotary forging. Microstructural characterization was performed using differential scanning calorimetry, high- and low-temperature X-ray diffraction (XRD) using a laboratory source and synchrotron XRD. Thus, it was possible to obtain the phase transformation characteristics of the material: the transformation temperatures and the transformation sequence. Proposed thermomechanical processing is intended for production of bars and wires that will be subsequently drawn to get thin wires, for different applications, including orthodontic arch wires. © *2017 International Centre for Diffraction Data*. [doi:10.1017/S0885715617000549]

Key words: rotary hot forging, X-ray diffraction, phase transformation, NiTi alloy, microstructural characterization

I. INTRODUCTION

Owing to their functional properties (shape memory effect and superelasticity), NiTi alloys are very interesting and appealing materials, with applications in medicine, civil engineering, and aerospace (Ramaiah *et al.*, 2005; Mohd Jani *et al.*, 2014).

The singular characteristics of NiTi alloys with composition close to equiatomic are a result of the presence of two phases: austenite (*Strukturbericht* designation: *B*2; space group $Pm\bar{3}m$), stable at a higher temperature, and martensite (*Strukturbericht* designation: *B*19'; space group $P2_1/m$), stable at a lower temperature. In some circumstances, an intermediate *R*-phase (space group $P\bar{3}$) may appear. In the following text, austenite, martensite, and *R*-phase will be designated by *B*2, *B*19', and *R*, respectively. Transformation temperatures in these alloys may be strongly affected by the Ni/Ti ratio of *B*2. The superelastic behavior, relevant for the orthodontic application, is a consequence of the stress-induced transformation $B2 \Leftrightarrow B19'$.

The manufacture of these materials is complex, since a variation of the chemical composition and the presence of impurities (e.g. C or O) can drastically change the characteristics of the material (Chu *et al.*, 1996; Frenzel *et al.*, 2007; Otubo *et al.*, 2008). The biggest challenges throughout its processing are the control of the metal matrix composition (ratio Ni/Ti) and the impurity content, such as the carbon and the oxygen, that can give rise to carbide (TiC) and oxide (Ti_4Ni_2O and Ti_2O) inclusions (Funakubo, 1987; Chu *et al.*, 1996; Otsuka and Ren, 2005; Frenzel *et al.*, 2007; Khamei and Dehghani, 2010a, 2010b). The presence of carbon or oxygen does not have a direct effect on the transformation temperature; rather, both elements preferentially combine with Ti to form stable compounds, leaving the matrix Ni rich and therefore resulting in a reduction of the transformation temperatures (Chu *et al.*, 1996; Frenzel *et al.*, 2007, 2010).

Understanding the behavior of these materials during their manufacturing process is important, especially during the hot deformation steps, such as forging (Dehghani and Khamei, 2010a, 2010b). During the hot deformation, cracking may occur as a result of compressive stresses and the presence of inclusions from the previous casting process (Otubo *et al.*, 2006).

The complexity of the process requires a verification of the functional properties after the applied thermomechanical treatment. The workability of these alloys decreases significantly for temperatures below 800 °C. These difficulties during the hot deformation are related to brittleness and notch sensitivity (Morakabati *et al.*, 2011a, 2011b). So, it is necessary: (i) to optimize the hot forging temperature in order to get the best hot workability and (ii) to guarantee that the metal matrix composition will ensure the stability of *B*2 in the working temperature range required for orthodontic application, between room temperature and oral temperature (~310 K).

[a)]Author to whom correspondence should be addressed. Electronic mail: pf.rodrigues@campus.fct.unl.pt

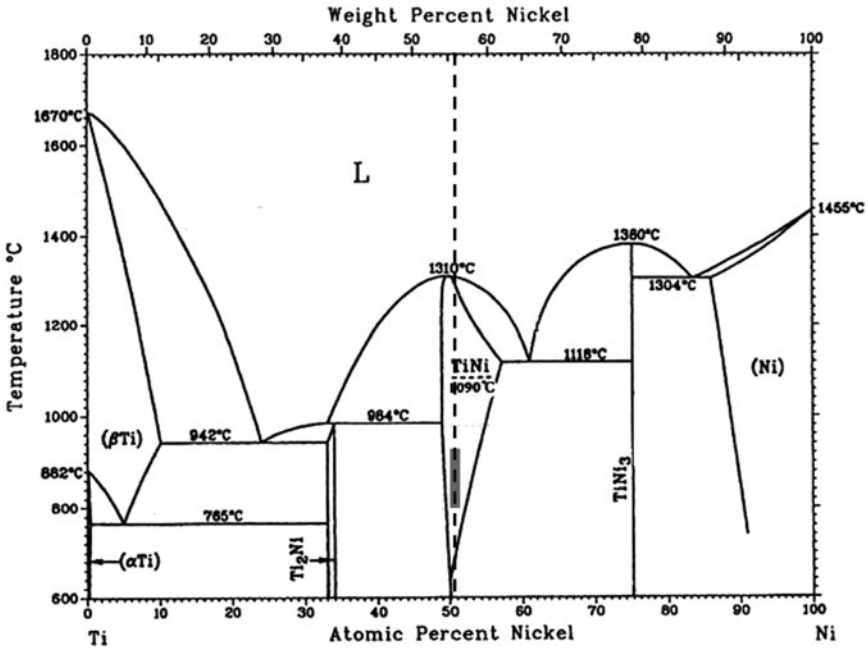

Figure 1. The Ni–Ti phase diagram (adapted from Massalski *et al.*, 1990). The dotted line corresponds to the composition of the alloy used in this study, and the gray bar marks the temperature range used for the hot working of this class of alloys (800 and 950 °C).

A few studies have been devoted to the deformation maps of NiTi alloys K (Ramaiah *et al.*, 2005; Dehghani and Khamei, 2010a, 2010b; Khamei and Dehghani, 2010a, 2010b; Morakabati *et al.*, 2011a, 2011b; Yeom *et al.*, 2014).

The aim of the present work is to study the processing route of a Ni-rich NiTi alloy after the first step of rotary hot forging from a processing sequence comprising casting by vacuum induction melting (VIM), remelting, and six steps of deformation (four steps of hot forging and two steps of cold forging). Figure 1 shows the Ni–Ti phase diagram (Massalski *et al.*, 1990). The composition of the Ni-rich NiTi alloy used in this study (Ni51.03 at.%–Ti48.97 at.%) is referenced by a dashed line, and the typical range of temperatures used for hot working is highlighted on the composition line.

In order to use this material for orthodontic wires production, it is required to optimize the hot workability of the material and to ensure the superelastic behavior close to oral temperature (310 K) at all the stages of the process.

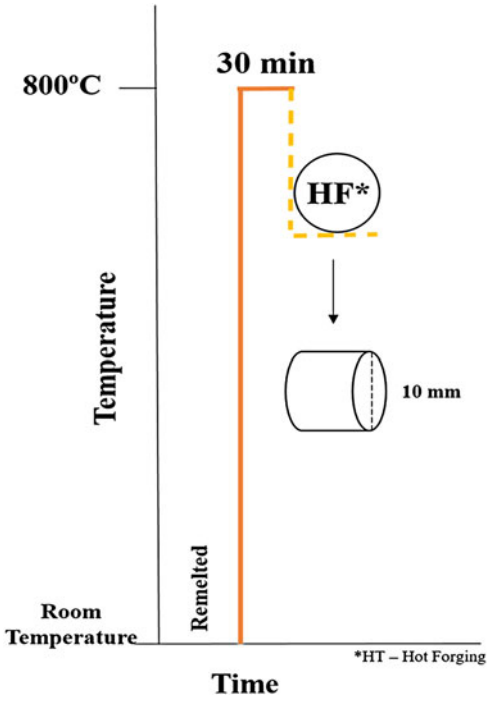

Figure 2. (color online) Schematics of the first step of thermomechanical process used in the present study.

II. EXPERIMENTAL

A. Material

The sample studied in the present work was obtained from an ingot produced in a VIM furnace under argon atmosphere using a graphite crucible. Subsequently, the ingot was subdivided into smaller pieces, about 90 g each, using electroerosion technique, in order to further recast in the arc melting furnace under argon atmosphere with previous vacuum and argon purge sequence. After being remelted, the ingot was then heated to 800 °C for 30 min. It was then submitted to hot forging, as shown in Figure 2 followed by a slow cooling to room temperature. In the present work, it was studied in the 1F (first hot forging, immediately after the remelting step) sample (Figure 2) (Table I).

The overall chemical composition of the material used in this investigation was determined by wavelength dispersion spectroscopy (WDS): 49.76 at.% of Ni, 47.83 at.% of Ti, 1.88 at.% of O, and 0.51 at.% of C. The following formula [see Eq. (1)] (Otsuka and Wayman, 1998) has been used for the correction of the effective Ni and Ti content in the metal matrix, taking into account the oxides and carbides formation:

$$\%\text{at.Ni}(e) = \frac{(\%\text{at.Ni} - 0.5\%\text{at.O}) \times 100}{[(\%\text{at.Ni} - (0.5 \times \%\text{at.O})] + [(\%\text{at.Ti} - \%\text{at.C} - (0.25 \times \%\text{at.O})]} \quad (1)$$

Using this formula, the final composition of the metal matrix was estimated to be 48.97 at.% of Ti and 51.03 at.% of Ni.

https://doi.org/10.1017/S0885715617000549 Published online by Cambridge University Press

TABLE I. Characteristics of the samples extracted for this study.

Sample	%at Ni	Diameter (mm)	Thickness (mm)
Remelting	51.03	18	5
1F first hot forging	51.03	10	3

B. Methods

The characterization of the transformation temperatures was performed by differential scanning calorimetry (DSC) and the structural characterization by X-ray diffraction (XRD).

For the DSC analysis, a DSC 204 F1 Phoenix was used, with thermal cycles from −150 to 150 °C and heating/cooling rate of 10 K min^{-1}. Before examination by DSC and XRD, the samples (~42 mg) were cut with a low-speed diamond saw and then chemically etched (10 vol% HF + 45 vol% HNO_3 + 45 vol% H_2O) in order to remove the oxide, as well as the layer deformed by the cutting operation.

For the XRD analysis, a laboratory source and synchrotron XRD (SXRD) was used.

The laboratory source was a Bruker X-ray diffractometer (Cu$K\alpha$ radiation). The non-ambient temperature measurements were performed, using a TTK-450 chamber (from Anton Paar), in the range −120 to +120 °C at intervals of 10 °C, during heating and cooling. The 2θ scans covered the range from 36° to 50° ($\delta 2\theta = 0.04°$; acquisition 1 s per point), so that the $B2$ (110) diffraction peak was observed, as well as other neighboring peaks from $B19'$. The texture measurements were performed with an Eulerian Cradle ($0 < \chi < 69$, $\delta\chi = 3$; $0 < \phi < 360°$, $\delta\phi = 3°$) for the (110), (200), and (211) $B2$ diffraction peaks.

The SXRD experiment was performed in transmission mode using a disc-shaped sample (18 mm diameter for remelting sample and 10 mm diameter for the 1F sample). It was performed at beamline P07 High-Energy Materials Science (HEMS) of Petra III/DESY, using a wavelength of 0.1426 Å (87 keV); a beam spot 200 × 200 μm^2 was used to scan the samples along a diameter (45 points) and a two-dimensional (2D) detector Mar345 was placed at 1.35 m from the sample. The raw 2D images were treated using Fit2D program in order to calculate the individual XRD patterns by integration from 0° to 360°.

For the XRD measurement, the identification of the diffraction peaks was based on the International Centre for Diffraction Data (ICDD) database. The samples (disc-shaped) used for XRD and SXRD were cut perpendicular to the longitudinal direction of the initial rod.

The XRD and DSC techniques were used in this work to check the structural state of the material and its transformation

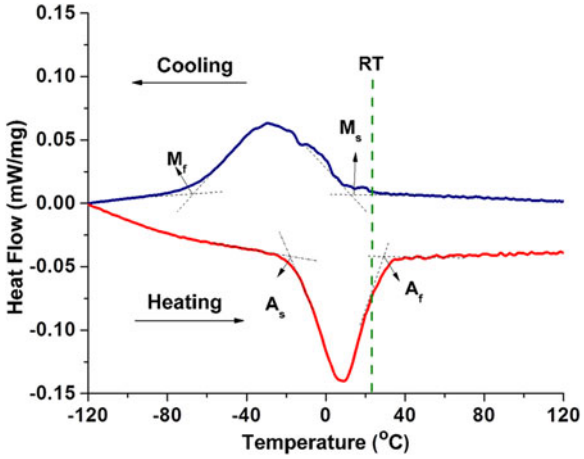

Figure 4. (color online) DSC curve of 1F sample.

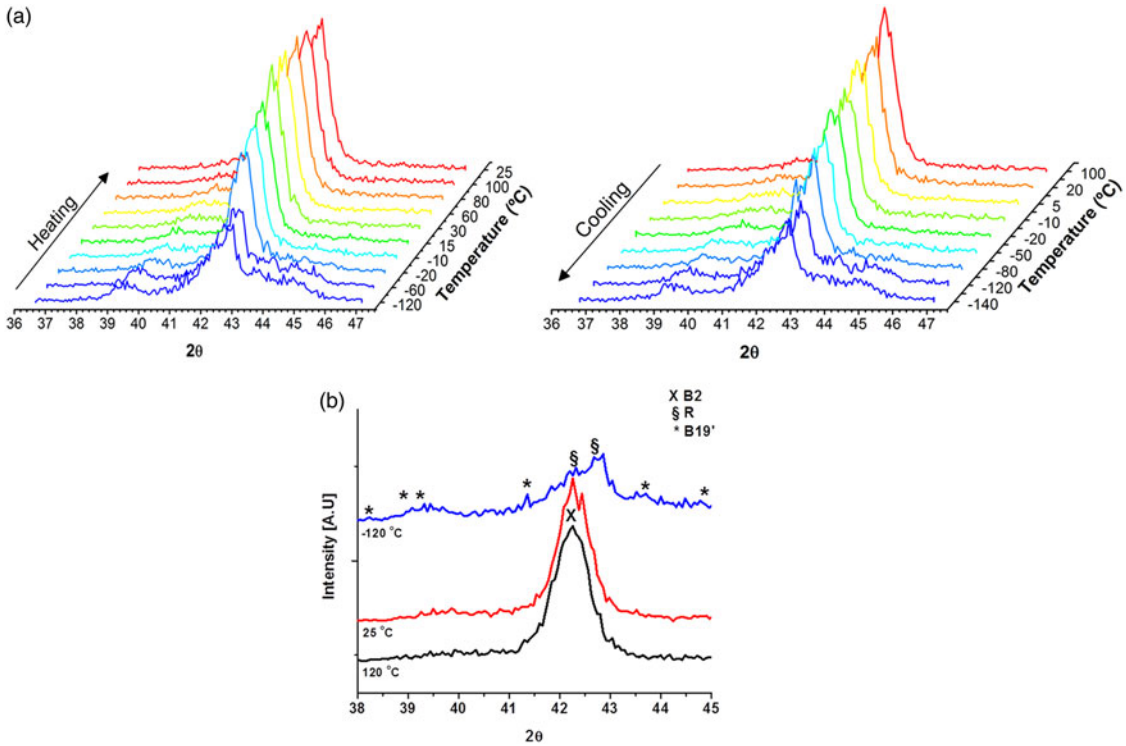

Figure 3. (color online) XRD results at high/low temperature: during heating and cooling, between −120 and 120 °C (a) separate diffractograms for three different temperatures (b).

https://doi.org/10.1017/S0885715617000549 Published online by Cambridge University Press

TABLE II. Phase transformation temperatures in °C

	Cooling (°C)			Heating (°C)		
	M_s	M_p	M_f	A_s	A_p	A_f
1F	7.2	−29.4	−59.0	−15.1	9.2	27.5

characteristics. The XRD results give a precise identification of the phases that are present but do not allow a precise definition of the transformation temperatures, because of the temperature steps of 10 °C between successive holdings. On the other hand, the DSC technique gives a precise definition of the transformation temperature ranges but does not always provide a clear identification of the individual phase transformations because of partial overlapping of transformation peaks. The SXRD also gives a local (0.2×0.2 mm^2) structural information, but restricted to room temperature. The three techniques provide complementary information about the structural/phase characteristics of the material.

III. RESULTS AND DISCUSSION

The XRD results show that a two-step phase transformation is taking place during cooling ($B2 \rightarrow R \rightarrow B19'$) and heating ($B19' \rightarrow R \rightarrow B2$) cycles (Figure 3).

For the higher temperature (above to 25 °C), the $B2$ (110) is clearly visible [Figure 3(b) – heating].

During cooling, under 25 °C, there is an abrupt decrease of the $B2$ (110) peak intensity, and two peaks associated to R-phase, close to $B2$ (110) peak, are noticed. During further cooling, other peaks associated to $B19'$ appear [Figure 3(a) – cooling].

The transformation temperatures were obtained by DSC analysis (Figure 4): the values of transformation temperatures are shown in Table II: austenite start and finish (A_s and A_f),

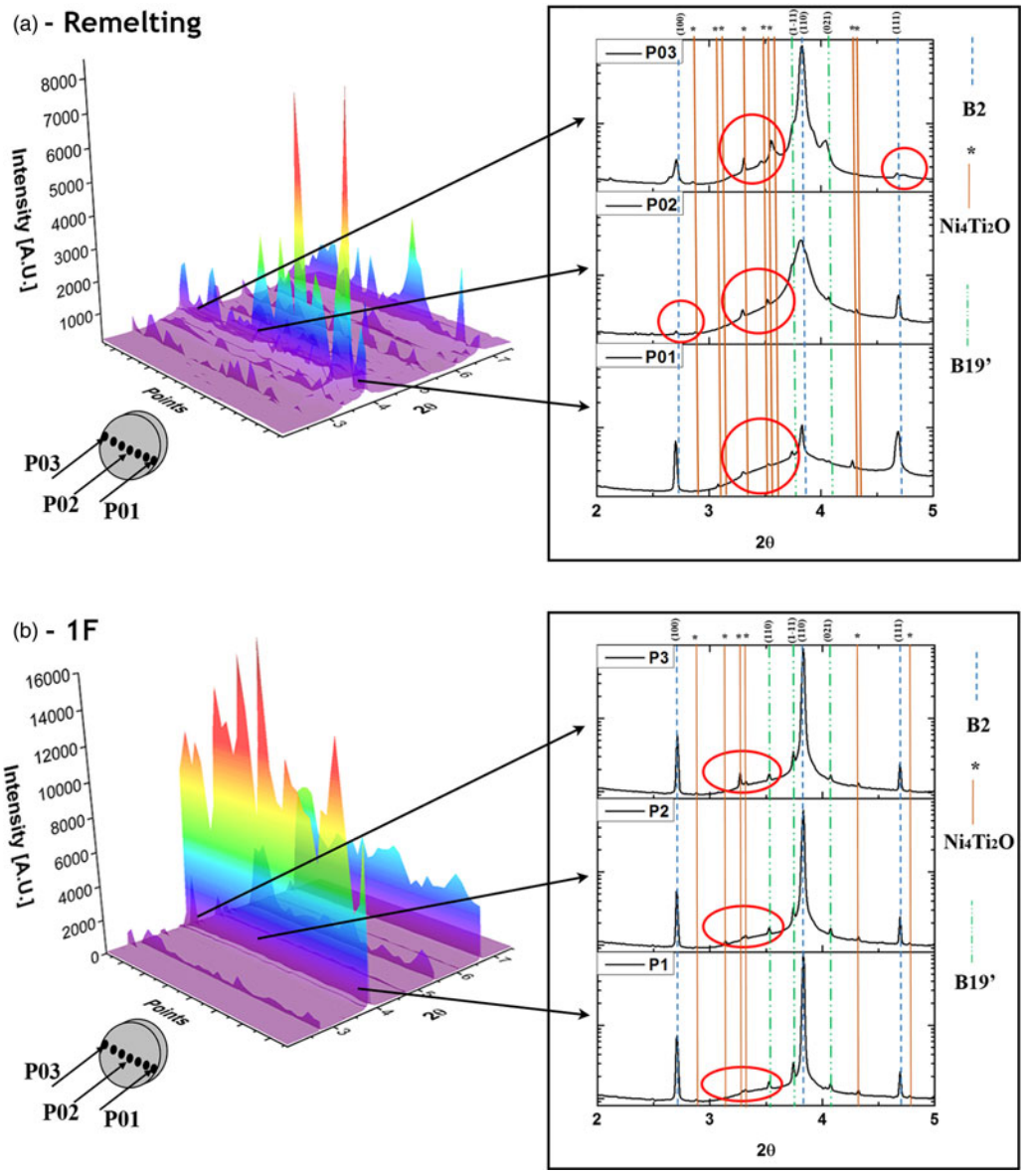

Figure 5. (color online) SXRD patterns at room temperature for the sample along the radial direction. (a) Remelting; (b) first step of hot forging (1F). The 3D XRD patterns on the left group represent the data obtained from 45 points along the diameter for each disc-shaped sample. To the right, three diffraction patterns are plotted amongst these 45 points: P01 and P03, close to the edge of the disc, and P02 at the center.

https://doi.org/10.1017/S0885715617000549 Published online by Cambridge University Press

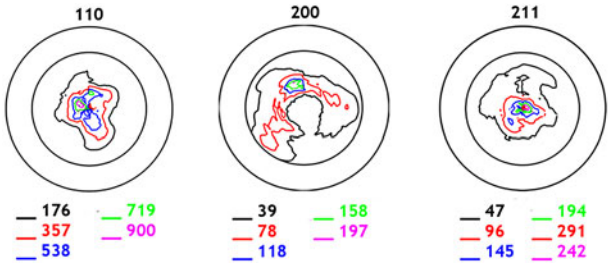

Figure 6. (color online) Pole figures of sample 1F.

during heating, and martensite start and finish (M_s and M_f), during cooling. In Figure 4, room temperature is highlighted with a vertical green line, showing that the sample is austenitic slightly above room temperature.

The DSC result shows only one transformation peak on heating and on cooling, suggesting that $B2 \Leftrightarrow B19'$ takes place in one single step, but the XRD results clearly show that the intermediate *R*-phase is formed. Thus, from XRD results, we may conclude that, during cooling/heating, there is a two-step phase transformation ($B2 \leftrightarrow R \leftrightarrow B19'$). This piece of information is not evident in DSC results, but it is consistent with the partial overlap of the temperature ranges of DSC peaks during cooling and heating, because of the smaller thermal hysteresis of the $B2 \leftrightarrow R$.

Figure 5 shows the schematic of the measurement along the radial direction using SXRD. In this scheme, we have isolated three diffraction patterns amongst the 45 points.

The SXRD results show an austenitic structure for all points analyzed (Figure 5). This result is consistent with the DSC analysis and the conventional (laboratory source) XRD result obtained at room temperature. The positions of the Ni_4Ti_2O peaks are highlighted with a circle (Figure 5). It is possible to observe that, for both samples, we have very different intensities for the *B*2 peaks. This fact could be associated with the very heterogeneous microstructure after the first hot-forging step (four hammer forging).

Pole figures (Figure 6) resulting from texture measurements do not indicate a fiber texture, as it is expected to happen at this step of the processing.

IV. CONLCUSIONS

The analysis of the DSC and XRD results for the first step of the thermomechanical process resulted on:

- the temperature A_f (austenite finish) is close to room temperature; this is relevant for the material to show austenite phase at oral temperature and, thus, show the superelastic behavior required for the application in orthodontic arch wires; this good expectation in terms of functional characteristics was observed after the first step of hot forging, although a notorious microstructural heterogeneity has been identified by SXRD results;
- the austenite ↔ martensite phase transformation takes place in two steps ($B2 \leftrightarrow R \leftrightarrow B19'$);
- the preferential orientation that is present in the rods at the end of the first step of hot forging does not show a fiber texture.
- the XRD results show that, although the material overall behavior is favorable to the expected superelastic behavior, the presence of oxides compromises the hot workability required for further steps of deformation.

These preliminary results show that the chemical composition ensuring the adequate functional properties has been approached, but the casting/remelting steps need to be improved in order to decrease the impurities content (C and O), thus ensuring that a significative improvement of the hot workability will be reached. Further work is currently following this trend.

ACKNOWLEDGMENTS

P.R., F.M.B.F, and J.P.O acknowledge the funding of CENIMAT/I3N by COMPETE 2020, through FCT, under the project UID/CTM/50025/2013. A.S.P, S.B.R, and P.R. acknowledge the funding of CAPES (APQ-1 2009/02 E-26/110.414/2010, APQ-1 2011-2 E-26/110.269.2012, E-26/111.435/2012 – CsF/ Brazil – BEX 11943-13-0) and CNPq (research productivity scholarship PQ-2 – Process 307798/2015-1). The authors thank Professor J. Otubo and postgraduates J.P. Toseti and G.H.T.A. da Silva, for donating the starting materials, and support in the use of the infrastructure of the Institute of Aeronautical Technology to achieve the melting and forging process conditions adopted in this work.

Chu, C. L., Wu, S. K., and Yen, Y. C. (**1996**). "Oxidation behavior of equiatomic TiNi alloy in high temperature air environment," Mater. Sci. Eng. A **216**, 193–200.

Dehghani, K. and Khamei, A. A. (**2010a**). "Hot deformation behavior of 60Nitinol ($Ni_{60\ wt\%}$–$Ti_{40\ wt\%}$) alloy: experimental and computational studies," Mater. Sci. Eng. A **527**, 684–690.

Dehghani, K. and Khamei, A. A. (**2010b**). "Modeling the hot-deformation behavior of Ni60 wt%–Ti40 wt% intermetallic alloy," J. Alloys Compd. **490**, 377–381.

Frenzel, J., Zhang, Z., Somsen, C., Neuking, K., and Eggeler, G. (**2007**). "Influence of carbon on martensitic phase transformations in Niti shape memory alloys," Acta Mater. **55**, 1331–1341.

Frenzel, J., George, E. P., Dlouhy, A., Somsen, Ch., Wagner, M. F.-X., and Eggeler, G. (**2010**). "Influence of Ni on martensitic phase transformations in NiTi shape memory alloys," Acta Mater. **58**, 3444–3458.

Funakubo, H. (**1987**). *Shape Memory Alloys* (Science Publishers, New York, Gordon and Breach), Vol. **1**.

Khamei, A. and Dehghani, K. (**2010a**). "Microstructural evolution during the hot deformation of Ti-55Ni (at. pct) intermetallic alloy," Metall. Mater. Trans. A **41**, 2595–2605.

Khamei, A. A. and Dehghani, K. (**2010b**). "A study on the mechanical behavior and microstructural evolution of Ni60 wt%–Ti40 wt% (60Nitinol) intermetallic compound during hot deformation," Mater. Chem. Phys. **123**, 269–277.

Massalski, T. B., Okamoto, H., Subramanian, P. R., and Kacprzak, L. (Eds.) (**1990**). *Binary Alloy Phase Diagrams* (ASM International 2874, Materials Park, OH), 2nd ed., Vol. **3**.

Mohd Jani, J., Leary, M., Subic, A., and Gibson, M. A. (**2014**). "Review: a review of shape memory alloy research, applications and opportunities," Mater. Des. **56**, 1078–1113.

Morakabati, M., Kheirandisha, Sh., Aboutalebia, M., Karimi Taherib, A., and Abbasic, S. M. (**2011a**). "A study on the hot workability of wrought NiTi shape memory alloy," Mater. Sci. Eng. A **528**, 5656–5663.

Morakabati, M., Aboutalebi, M., Kheirandish, Sh., Karimi Taheri, A., and Abbasi, S. M. (**2011b**). "High temperature deformation and processing map of a NiTi intermetallic alloy," Intermetallics **19**, 1399–1404.

Otsuka, K. and Ren, X. (**2005**). "Physical metallurgy of Ti–Ni-based shape memory alloys," Prog. Mater. Sci. **516**, 669.

https://doi.org/10.1017/S0885715617000549 Published online by Cambridge University Press

Otsuka, K. and Wayman, C. M. (**1998**). *Shape Memory Materials* (Cambridge University Press, Cambridge, UK).

Otubo, J., Rigo, O. D., Moura Neto, C., and Mei, P. R. (**2006**). "The effects of vacuum induction melting and electron beam melting techniques on the purity of NiTi shape memory alloys," Mater. Sci. Eng. **438–440**, 679–682.

Otubo, J., Rigo, O. D., Coelho, A. A., Neto, C. M., and Mei, P. R. (**2008**). "The influence of carbon and oxygen content on the martensitic transformation temperatures and enthalpies of NiTi shape memory alloy," Mater. Sci. Eng. A **481–482**, 639–642.

Ramaiah, K. V., Saikrishna, C. N., and Bhaumik, S. K. (**2005**). "Processing of Ni-Ti Shape Memory Alloy Wires," Int. Conf. of Smart Materials Structures and Systems 2005:SC141.

Yeom, J.-T., Kim, J. H., Hong, J.-K., Kim, S. W., Park, C.-H., Nam, T. H., and Lee, K.-Y. (**2014**). "Hot forging design of as-cast NiTi shape memory alloy," Mater. Res. Bull. **58**, 234–238.

https://doi.org/10.1017/S0885715617000549 Published online by Cambridge University Press